WILEY | Hindawi

Research Article

Risk Assessment of Annular Pressure Caused by Tubing Leakage in Offshore Gas Wells with High CO_2

Ninghui Dou,[1,2] Zhiqiang Hu ,[2] Zhiyuan Wang ,[1] Hanpin He,[2] and Shunhui Yang[2]

[1]*School of Petroleum Engineering, China University of Petroleum (East China), Qingdao 266580, China*
[2]*SINOPEC Research Institute of Petroleum Engineering Co., Ltd., Beijing 102206, China*

Correspondence should be addressed to Zhiyuan Wang; wangzy1209@126.com

CO_2 sequestration is a kind of technology that can effectively mitigate the greenhouse effect, and the wellbore integrity of the storage system is the key issue to ensure successful CCUS. Failure to timely diagnose tubing leakage in offshore gas wells with high CO_2 will lead to annular pressure risk and wellbore corrosion problems. The annular pressure caused by tubing leakage is characterized by high pressure and rapid rise rate, resulting in wellhead jacking, gas leakage, and wellbore structure corrosion, which has become the main cause of wellbore integrity failure in offshore gas wells. Therefore, a model of heat and mass transfer and distribution in offshore gas wells was established firstly, and the physical process of gas leakage and accumulation was described based on the pinhole model and the principle of gas PVT characteristics and volume compatibility. The results show that the depth and equivalent size of the leakage point are two important factors affecting the pressure rise process and leakage rate. Taking case well parameters as an example, after inversion calculation, the annulus pressure in case well was 23.0 MPa, the leakage point equivalent diameter was 2.3 mm, the maximum leakage rate was 0.30 m^3/min, and the wellbore safety risk is relatively high. Mechanical repair and chemical plugging agent are recommended to seal the tubing leakage. These risk assessment technologies provide reference for wellbore integrity design and management to reduce CO_2 leakage risk caused by wellbore integrity failure.

1. Introduction

With the development of offshore oil and gas industry, most of the offshore gas well production faces high temperature, high pressure, and high corrosive gas containing downhole environment, and the phenomenon of abnormal pressure carrying in the annulus column was gradually increasing [1–6]. According to the U.S. Bureau of Mines, up to 60% of gas wells have annular pressure buildup phenomenon, and the failure of oil casing column leakage accounts for more than 50%, becoming the primary factor. Once a tubing leak occurs, the tubing-casing annular pressure rises sharply, accompanied by corrosive media such as hydrogen sulfide gas and carbon dioxide gas in the natural gas of the marine well fleeing into the annulus, the degree of leakage expands, and the wellbore barrier fails. If the annulus gas with high CO_2 leaks to the surface, it not only causes the CO_2 pollution and makes environmental problems but also leads to wellbore scrapping and endangers the lives and property of personnel. At present, continuous annular pressure analysis mainly focuses on the casing annular pressure caused by cement sheath failure [7–10], usually using formation gas as the source of leakage, using the cement sheath as the transport channel, using the PVT conservation relationship to calculate the pressure value, and controlling the annular pressure by optimizing the cement sheath system. Some scholars have also conducted studies on the characteristics of pressure changes under gas-driven recovery tubular column puncture [11–14] and completion tubular column leakage [15–18]. However, the annular pressure caused by tubing leakage is different from the pressure caused by cement sheath integrity failure, which is mainly reflected in the difference of gas leakage source, leakage, and gathering process, which is not conducive to carry out relevant risk prediction and control measure research. Therefore, how to use production data such as wellbore pressure, temperature, flow rate, gas components, and liquid level to make accurate judgments on the extent of

tubing-casing annulus leakage through surface diagnostic techniques has become a research challenge. This paper predicts the depth of the leak point based on the pressure balance principle, describes the pressurization process of gas leakage using a small-hole leakage model, analyzes the influence of leak point parameters on the change pattern of annular pressure, and summarizes four types of typical pressure initiation patterns of tubing-casing annular pressure by combining the characteristics of annular pressure relief recovery test curves. It provides technical support for the integrity evaluation of offshore production wells, well repair, oil recovery operations, and the management of CO_2 leakage risk.

2. Wellbore Heat Mass Transfer and Temperature-Pressure Coupling Model

The difference in temperature and pressure inside and outside the tubular column of an offshore production well is the initial driver of gas leakage. Due to the relatively high temperature of the fluid extracted from the formation, during the upward transport along the wellbore, the high-temperature formation fluid will continue to dissipate heat to the low-temperature medium around the wellbore, resulting in a constant change in temperature within the production tubular column with well depth [19]. As shown in Figure 1, a microelement body of length dz is taken within the tubing column and the conservation of momentum and compliance with the energy conservation relationship within the microelement, and the two conservation equations are shown in

$$\begin{cases} \dfrac{dp}{dz} + \rho_f g \sin\theta + f\dfrac{\rho_f v_f^2}{d_{tn}} + \rho v_f \dfrac{dv_f}{dz} = 0, \\ C_f \dfrac{dT_f}{dz} + v_f \dfrac{dv_f}{dz} + \dfrac{1}{\rho_f}\dfrac{dp}{dz} + g\sin\theta + \dfrac{1}{w_f}\dfrac{dQ}{dz} = 0, \end{cases} \quad (1)$$

where p is the pressure (Pa), ρ_f is the gas density in the tubing (kg/m^3), g is the gravitational acceleration (m/s^2), θ is the well slope angle (°), f is the friction coefficient (factorless), v_f is the gas flow rate (m/s), C_f is the gas-specific heat capacity (J/(kg-°C)), T_f is the gas temperature (°C), w_f is the gas mass flow rate (kg/s), and Q is the wellbore radial heat flow rate (J/s).

The friction coefficient in Equation (1) is calculated as shown in the following equation:

$$\begin{cases} f^{-0.5} = -2\log\left[\dfrac{R_a}{3.715d_{tn}} + \left(\dfrac{6.943}{Re}\right)^{0.9}\right], \\ Re = \dfrac{\rho_f v_f d_{tn}}{\mu}, \end{cases} \quad (2)$$

where R_a is the oil pipe roughness (m), d_{tn} is the oil pipe inner diameter (m), Re is the Reynolds number (dimensionless), and μ is the gas viscosity (Pa-s).

The heat transfer within the wellbore and between the wellbore and the formation is in accordance with the principle of radial heat flow conservation [20, 21], as shown in

$$dQ = dQ_{rw} = dQ_{rf}, \quad (3)$$

$$\begin{cases} dQ_{rw} = \dfrac{T_f - T_h}{R_{to}}dz, \\ dQ_{rf} = \dfrac{2\pi\lambda e(Th - Te)}{TD}dz, \end{cases} \quad (4)$$

where Q_{rw} is the radial heat flow rate from the center of the tubing to the edge of the wellbore (J/s), Q_{rf} is the radial heat flow rate from the edge of the cement sheath to the formation (J/s), T_h is the temperature at the edge of the wellbore (°C), R_{to} is the radial heat transfer thermal resistance in the wellbore (m-°C/W), λ_e is the formation thermal conductivity (W/(m-°C)), T_e is the formation temperature (°C), and T_D is the dimensionless stratigraphic temperature (dimensionless).

Combining Equations (3) and (4) yields the radial heat flow rate as shown in

$$\dfrac{dQ}{dz} = \dfrac{2\pi\lambda_e(T_e - T_f)}{T_D + 2\pi\lambda_e R_{to}}. \quad (5)$$

The transient factorless temperature in Equation (3) is shown in

$$T_D = \begin{cases} 1.1281\sqrt{t_D}\left(1 - 0.3\sqrt{t_D}\right), & t_D \leq 0.5, \\ \ln\left(2\sqrt{t_D}\right)\text{-}0.2886 + \dfrac{1}{4t_D}\left[1 + \left(1\text{-}\dfrac{1}{\omega}\right)\ln\left(4t_D\right) + 0.5772\right], & 0.5 < t_D \leq 20, \\ \ln\left(2\sqrt{t_D}\right) - 0.2886, & 20 < t_D, \end{cases} \quad (6)$$

$$tD = \dfrac{t\alpha e}{rw^2}, \quad (7)$$

where t_D is the dimensionless time (dimensionless), ω is the ratio of borehole-specific heat capacity to formation-specific heat capacity (dimensionless), t is the time (s), α_e is the formation heat spreading coefficient (m^2/s), and r_w is the borehole radius (m).

Substitute Equation (5) into Equation (1), and substitute the conservation of momentum relationship into the conservation of energy relationship; at this time, the pressure and temperature along the direction of the tube column are shown in

$$\begin{cases} \dfrac{dp}{dz} = -\left(\rho_f g\sin\theta + f\dfrac{\rho_f v_f^2}{2d_t} + \rho v_f\dfrac{dv_f}{dz}\right), \\ \dfrac{dT_f}{dz} = \dfrac{2\pi\lambda_e(T_{es} - T_f)}{W_f C_f(T_D + 2\pi\lambda_e R_{to})} + f\dfrac{v_f^2}{C_f d_{tn}}. \end{cases} \quad (8)$$

There is a coupling relationship between the temperature and pressure fields inside the oil pipe column. Therefore, a spatial segmentation method is used to obtain the temperature and pressure distribution within the tubular column. Firstly, the tubing is divided into segments of length $\triangle z$ along the direction from the bottom of the well to the wellhead, and the temperature and pressure are kept constant within the segments, and Equation (9) is obtained from Equation (8).
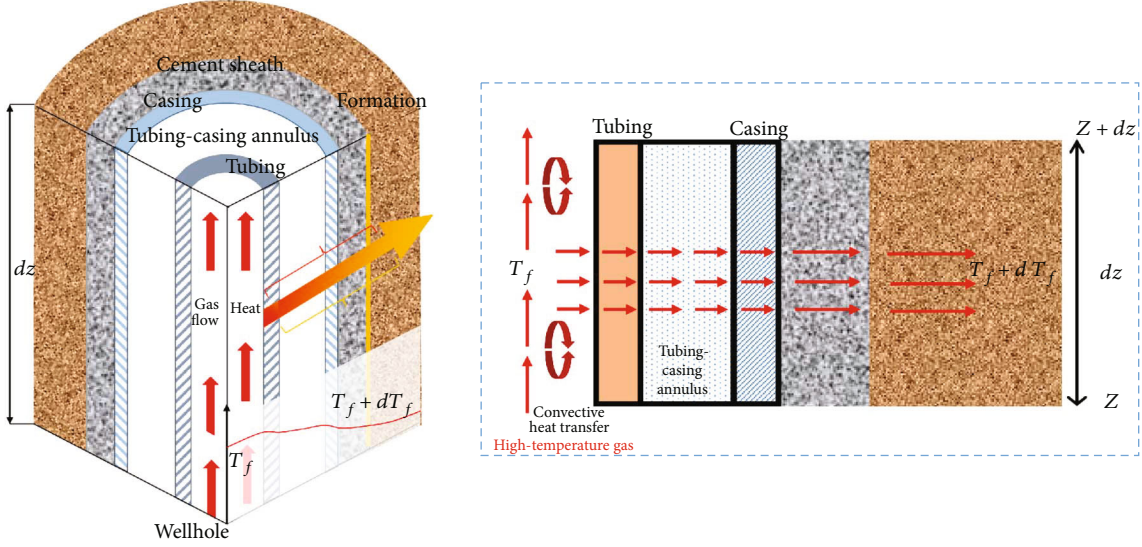
FIGURE 1: Schematic diagram of the physical process of heat transfer in the wellbore.

$$\begin{cases} p_f^{i+1}(t) = p_f^i(t) - \left(\rho_f^{i+1} g \sin\theta + f^{i+1} \dfrac{\rho_f (v_f^{i+1})^2}{2d_t} \right) \Delta z - \rho_t^{i+1} v_f^{i+1} \Delta v_f^{i+1}, \\[3mm] T_f^{i+1}(t) = \dfrac{1}{A + \Delta z} \left(A T_f^i(t) + \Delta z T_{es}^{i+1} + A \Delta z f^{i+1} \dfrac{(v_f^{i+1})^2}{C_f d_{tn}} \right), \end{cases}$$

$$(9)$$

where A is the calculated parameter, as shown in

$$A = \frac{w_f C_f [T_D + 2\pi \lambda_e R_{to}]}{2\pi \lambda_e},$$

$$(10)$$

where i is the segment number, $i = 1, 2, 3 \cdots \cdots$ (dimensionless), and $\triangle z$ is the segment length (m).

According to the PVT nature of the gas and the law of mass conservation, the velocity change and the gas density within each segment are shown in

$$\frac{dv_f}{dz} = -\frac{v_f}{\rho_f} \frac{d\rho_f}{dz} \longrightarrow \Delta v_f^{i+1} = \frac{v_f^{i+1}}{\rho_f^{i+1}} \frac{\rho_f^{i+1} - \rho_f^i}{\Delta z},$$

$$(11)$$

$$\rho_f^i = \frac{p_f^i M_g}{Z_g^i R T_f^i}.$$

$$(12)$$

The compression factor Z_g is temperature-pressure dependent and can be expressed by Ehsan's equation as shown in

$$\begin{cases} Z_g = \dfrac{A_1 + A_2 \ln p_r + A_3 (\ln p_r)^2 + A_4 (\ln p_r)^3 + A_5/T_r + A_6/T_r^2}{1 + A_7 \ln p_r + A_8 (\ln p_r)^2 + A_9/T_r + A_{10}/T_r^2}, \\[3mm] p_r = \dfrac{10^{-6} p_f}{4.666 + 0.103\gamma_g - 0.25\gamma_g^2}, \\[3mm] T_r = \dfrac{273.15 + T_f}{93.3 + 181\gamma_g - 7\gamma_g^2}, \end{cases}$$

$$(13)$$

where A_1, A_2, A_3, A_4, A_5, A_6, A_7, A_8, A_9, and A_{10} are the constants (dimensionless); p_r is the proposed comparison pressure (dimensionless); T_r is the proposed comparison temperature (dimensionless); and γ_g is the relative density of gas (dimensionless).

The gas viscosity is closely related to the temperature and can be expressed by the Sartland formular as shown in

$$\frac{\mu}{\mu_0} = \left(\frac{273.15 + T_f}{273.15 + T_0} \right)^{1.5} \frac{273.15 + T_0 + B}{273.15 + T_f + B},$$

$$(14)$$

where μ_0 is the measured viscosity of the gas (Pa-s), T_0 is the temperature corresponding to the measured viscosity (°C), and B is the constant, taken as 110.4.

3. Physical Model of Gas Leakage

After the failure of the tubular column of the offshore gas well under the effect of its own gravity, high temperature and pressure, and fluid corrosion, the gas enters the tubing-casing annulus through the leakage point of the tubular column, leaks from the inside of the tubular column to the outside annulus under the effect of the temperature and pressure difference between the inside and outside, and then floats and transports to the top of the annulus through the protective fluid of the annulus, forming a gas cavity (as shown in Figure 2). The whole physical process can be divided into three stages: tube column failure leakage, gas floating transport, and cavitation gathering and pressurization, as follows:

(1) After completion of a natural gas well, the annular wellhead pressure P_{co} should be zero, excluding the effect of wellbore temperature

(2) When a leak occurs in the production tubing column, driven by pressure, high-pressure oil and gas will flow into the annulus from the inside of the production tubing column. At the same time, this fluid

will compress the existing fluid in the annulus, causing the annulus wellhead pressure P_{c1} to rise

(3) And when the production pipe column and the pressure of the annulus on both sides of the leak point are balanced, the leak stops and the annular pressure P_{c2} rises to a steady state

(4) The wellbore pressure-depth distribution diagram shows that as fluid continues to leak into the annulus, the annular pressure profile gradually shifts to the right until the annular pressure P_{CL} at the leak point is equal to the production tubing column pressure P_{TL}

Therefore, the following modeling assumptions are made before the calculation:

(1) There is only one-dimensional stable fluid flow in the tubing

(2) Heat transfer in wellbore and between wellbore and formation conforms to the principle of conservation of radial heat flow

(3) The fluid thermodynamic properties of tubing are consistent at the same depth

(4) The leak point below the liquid column in the annulus and the height could be measured by surface equipment

(5) The model involves only one leak point

The temperature and pressure inside the tubing column are higher than the outer sleeve annulus, so the gas inside the column will leak into the sleeve annulus upon failure of the column integrity. The failure of the tubing column that causes sustained annular pressure is small, so the small-hole leakage model can be used to describe the leakage process of gas through the failure location. The small-hole model treats the flow as noncritical and critical, where the noncritical flow is related to the pressure inside and outside the leak point, while the critical flow is related to the internal pressure at the leak point only, as shown in

$$
Q_{Lg} = \begin{cases} C_o \dfrac{p_{fL} A_L}{\rho_{gs}} \sqrt{\dfrac{2k_g}{k_g - 1} \dfrac{M_g}{Z_g R T_{fL}} \left[\left(\dfrac{p_{aL}}{p_{fL}} \right)^{2/k_g} - \left(\dfrac{p_{aL}}{p_{fL}} \right)^{(k_g+1)/k_g} \right]}, & \text{CRE} < \dfrac{p_{aL}}{p_{fL}}, \\ C_o \dfrac{p_{fL} A}{\rho_s} \sqrt{\dfrac{M_g k_g}{Z_g R T_{fL}} \left(\dfrac{2}{k_g + 1} \right)^{(k_g+1)/(k_g-1)}}, & \text{CRE} \geq \dfrac{p_{aL}}{p_{fL}}. \end{cases}
$$
$$(15)$$

The critical pressure CRE is shown in

$$
\text{CRE} = \left(\dfrac{2}{k_g + 1} \right)^{k_g/(k_g-1)},
$$
$$(16)$$

where Q_{Lg} is the leak rate (nominal) (m³/s), C_o is the flow coefficient (dimensionless), p_{fL} is the pressure inside the leak point (Pa), A_L is the equivalent area of the leak point (m²), ρ_{gs} is the nominal density of the gas (kg/m³), k_g is the adiabatic index of the gas (dimensionless), M_g is the molar mass of the gas (kg/mol), Z_g is the compression factor (dimensionless), p_{aL} is the pressure outside the leak (Pa), T_{fL} is the temperature at the leak (K), and CRE is the critical pressure ratio (dimensionless).

According to Equation (15), the leak rate is related to the pressure inside and outside the leak point of the tubing column. The pressure inside the leak point is the internal pressure of the tubing column, while the external pressure consists of the pressure in the annulus and the pressure generated by the fluid inside the annulus, as shown in

$$
p_{aL} = \begin{cases} p_{an} + \rho_{ga} g h_L, & h_L \leq h_g, \\ p_{an} + \rho_{ga} g h_g + \rho_L g (h_L - h_g), & h_L > h_g, \end{cases}
$$
$$(17)$$

where p_{an} is the annular pressure (Pa), ρ_{ga} is the density of gas in the annulus (kg/m³), and ρ_L is the density of liquid in the annulus (kg/m³).

The gas density is lower than the annulus liquid, so it will float up from the leak point to the wellhead and finally gather in the annulus, so only the floating of the gas in the tubing-casing annulus liquid belongs to the intermediate process, and the final distribution state of the gas in the annulus is the factor that determines the size of the annular pressure. After the gas enters the annulus, it floats upward from the leak point to the wellhead and finally collects in the upper part of the annulus, in which the tubing-casing annulus conforms to the volume compatibility principle. Therefore, the volume relationship after the leak is shown in

$$
V_{ag} + V_{aL} + \Delta V_{aL} = V_{an} + \Delta V_{an},
$$
$$(18)$$

where V_{ag} is the volume of gas column in the annulus (m³), V_{aL} is the initial volume of liquid column in the annulus (m³), ΔV_{aL} is the volume change of liquid column in the annulus (m³), V_{an} is the volume of annulus (m³), and ΔV_{an} is the volume change of annulus (rigid in the annulus (m) and space is zero (m³)).

In the above equation, the volume of the annulus gas column is affected by temperature and pressure. Since the temperature of the annulus varies along the depth of the well, the gas volume is calculated by using the method of segment superposition, and the gas temperature within the segment is the same when the length is small enough. According to the PVT law for gases, the volume of the entire gas column is shown in

$$
V_{ag} = \dfrac{V_g}{M} \sum_{n=1}^{M} \dfrac{p_s T_{agn}}{p_{agn} T_s},
$$
$$(19)$$

where V_g is the cumulative gas leakage (standard condition) (m³), M is the number of segments (dimensionless), n is the annulus segment number (dimensionless), p_s is the standard condition pressure (Pa), p_s is the standard condition

(a) No Leakage
$P_{TL} > P_{CL}$

(b) Leakage
$P_{TL} > P_{CL}$

(c) Steady State
$P_{TL} = P_{CL}$

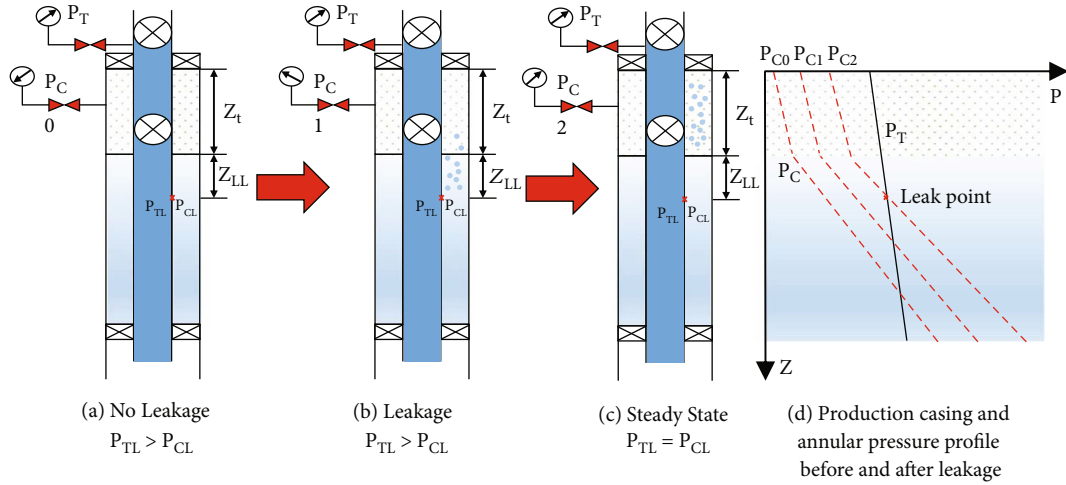(d) Production casing and annular pressure profile before and after leakage

FIGURE 2: Physical model of the gas leakage process.

temperature (K), T_{agn} is the annular temperature (K), and p_{agn} is the pressure in the annulus (Pa).

The volume change of the liquid occurs under the combined effect of temperature and pressure, as shown in

$$\Delta V_{aL} = V_{aL}\left(\Delta T_{aL}\alpha_p - 10^{-6}p_{an}K_T\right), \qquad (20)$$

where $\triangle T_{aL}$ is the average temperature change of the annular liquid (°C), α is the liquid isobaric expansion coefficient (°C^{-1}), K_T is the liquid isothermal compression coefficient (MPa^{-1}), and p_{an} is the annular pressure (Pa).

Equations (19) and (20) in the gas volume and liquid volume are affected by the change in the temperature of the annulus. According to the principle of radial heat flow conservation, the average temperature of the inner and outer sides of the annulus is taken as the annulus temperature, and the annulus temperature is shown in

$$\begin{cases} T_a = T_f - \dfrac{(R_{ao} + R_{ai})(T_f - T_h)}{2R}, \\ T_h = \dfrac{T_D T_f + 2\pi\lambda_e R_{to} T_e}{T_D + 2\pi\lambda_e R_{to}}. \end{cases} \qquad (21)$$

Correspondingly, for the average segmentation of the annular fluid, the average temperature change is shown in

$$\Delta T_{aL} = \frac{\sum_{y=1}^{N}\left(T_{aLy} - T_{esy}\right)}{N}, \qquad (22)$$

where T_a is the annulus temperature (°C), R_{ao} is the annulus outer to tubing thermal resistance (m·°C/W), R_{ai} is the annulus inner to tubing thermal resistance (m·°C/W), T_{es} is the annular initial temperature (°C), y is the annular liquid segment number (the no factor), and N is the total number of annulus liquid segments (no factor).

After obtaining the temperature, pressure distribution and variation, and gas leakage, substituting Equations (19)

and (20) into Equation (18) constitutes an equation for the annular pressure. In this case, there is a coupling between the annular gas leakage rate and the annular pressure in the relationship. For this reason, the total amount of gas entering the annular, when the pressure is unchanged for a shorter period of time, is shown in

$$V_g = V_{gs} + \sum_{j=1}^{sj} Q_{Lgj}\Delta t, \qquad (23)$$

where V_{gs} is the initial gas volume in the annulus (standard condition) (m^3), sj is the number of time segments (dimensionless), j is the time step number (dimensionless), and Δt is the time step (s).

The analysis shows that there is a coupling relationship between the temperature and pressure field inside the oil pipe column, and the total pressure and gas in the tubing-casing annulus also changes with time. Therefore, a spatial segmentation and time iteration method is used for the solution. Before a leak occurs, the liquid within the annulus undergoes thermal expansion to generate the confined annular pressure. Therefore, the initial conditions are shown in

$$\begin{cases} t = t_L, \\ T_f^1(t_L) = T_{esb}, \\ p_f^1(t_L) = p_b, \\ \Delta v_f^1 = 0, \\ p_{an}(t_L) = p_{tap}(t_L), \end{cases} \qquad (24)$$

where t_L is the time when the leak occurred (s), T_{esb} is the temperature at the bottom of the well (°C), p_b is the pressure at the bottom of the well (Pa), and p_{tap} is the pressure generated by thermal expansion of the annular fluid before the leak (Pa).

After obtaining the initial conditions, the gas physical parameters under the temperature-pressure conditions of

TABLE 1: Calculated parameters.

| Parameters	Numerical value	Parameters	Numerical value
Ground temperature gradient	0.02°C/m	Stratigraphic density	2.35 g/cm^3
Production layer temperature	150°C	Stratigraphic thermal diffusion coefficient	11.7×10^{-7} m^2/s
Production layer pressure	115 MPa	Thermal conductivity of strata	5.1 W/(m-°C)
Circumferential liquid density	1.2 g/cm^3	Oil pipe roughness	1.6×10^{-5} m
Thermal conductivity of annular liquid	0.62 W/(m-°C)	Isobaric expansion coefficient of annular liquid	0.00013°C^{-1}
Isothermal compression coefficient of annular liquid	0.00040 MPa^{-1}	Thermal conductivity of gases	0.025 W/(m-°C)
Specific heat capacity of produced gas	2310 J/(kg-°C)	Relative density of produced gas	0.75
Daily gas production capacity	40×10^4 m^3/d	Output gas viscosity	1.55×10^{-6} Pa-s
Adiabatic index of gas	1.29	Gas constants	8.3414
Cement sheath thermal conductivity	0.52 W/(m-°C)	Casing thermal conductivity	50.5 W/(m-°C)
Stratigraphic specific heat capacity	890 J/(kg-°C)	Leak point depth	3000 m
Space step	1 m	Time step	20 s
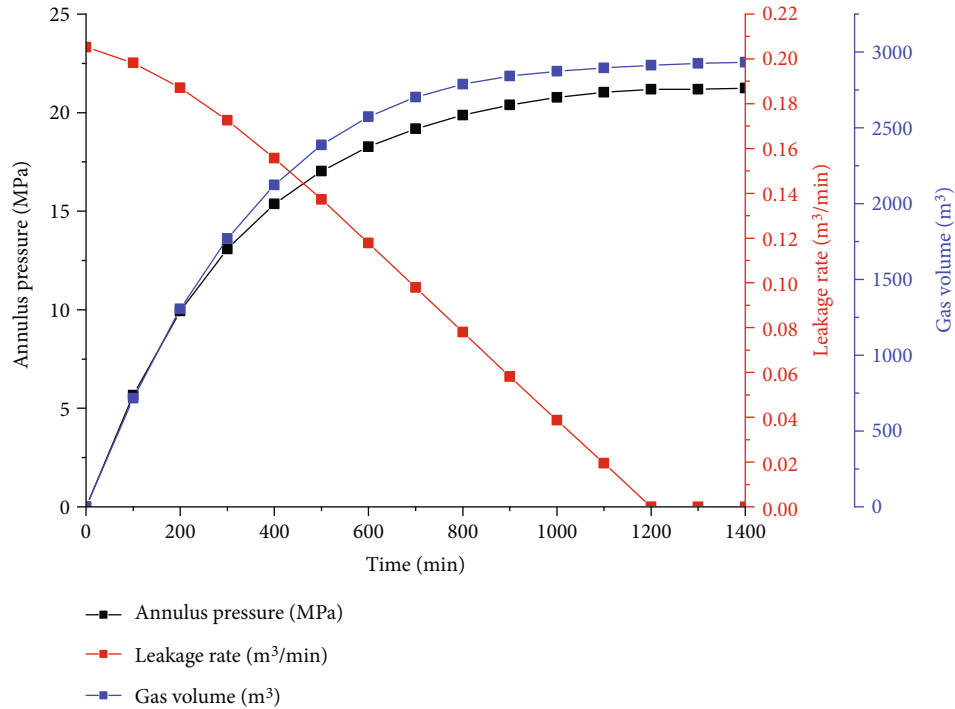
FIGURE 3: Circumstance pressure, leakage rate, and gas volume versus time after a leak occurs.

segment i are used to calculate the pressure temperature of each subsegment of segment $i + 1$, and then, the gas physical parameters of segment $i + 1$ are recalculated, and the difference between the two calculated rates is used as the rate change value, and then, the temperature pressure of the new segment $i + 1$ is solved, and the error analysis is performed with the previous one, and the calculation of the next subsegment up to the wellhead is continued after meeting the error. Then, calculate the leak rate according to the location of the leak point, obtain the volume of gas inside the annulus, and then solve for the annular pressure, after which make time continue and cycle the calculation until the ratio of pressure difference inside and outside the leak point reaches a predetermined value.

4. Case Study

The case well is a high-temperature and high-pressure well with gas reservoir temperature of 150°C, CO_2 content of 45%, and CO_2 partial pressure of 20.5 MPa. There is obvious sustained annular pressure in tubing-casing annulus. In order to avoid the damage to people and property which caused by the CO_2 leakage from the annulus, it is necessary to find an accurate diagnosis method for downhole leakage. The relevant calculated parameters are shown in Table 1.

As shown in Figure 3, the annular pressure and gas volume rose gradually after the leakage occurred, but the rising rate slowed down gradually. The tubing-casing annular
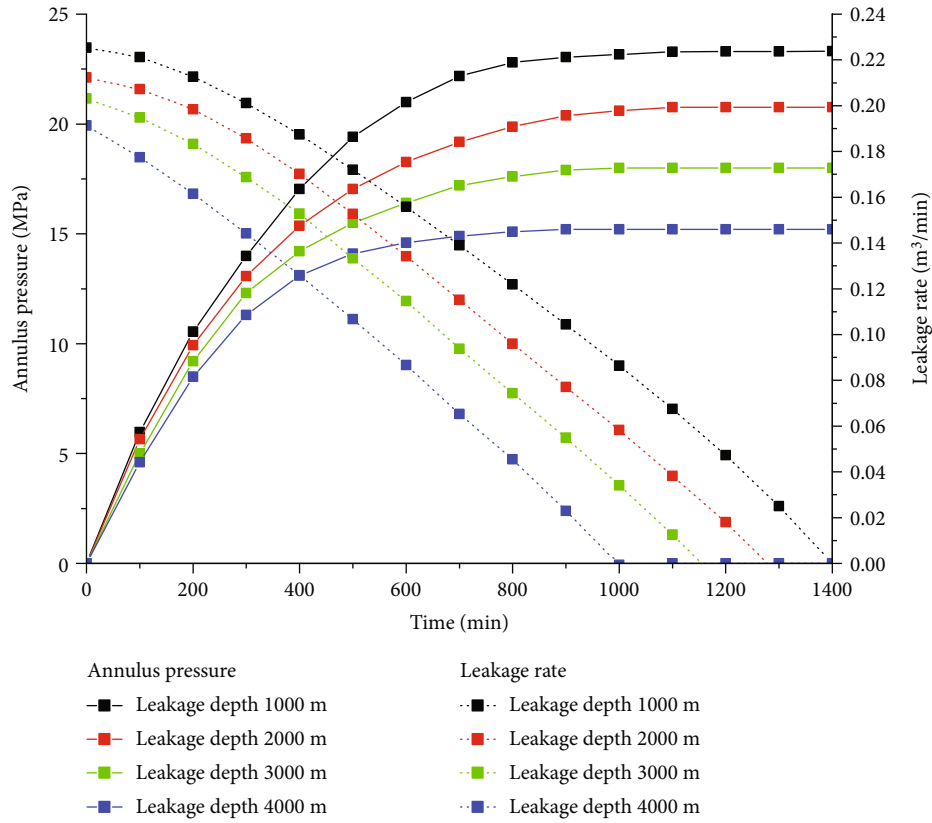
FIGURE 4: Circumstance pressure and leakage rate change law under different leakage point depth.
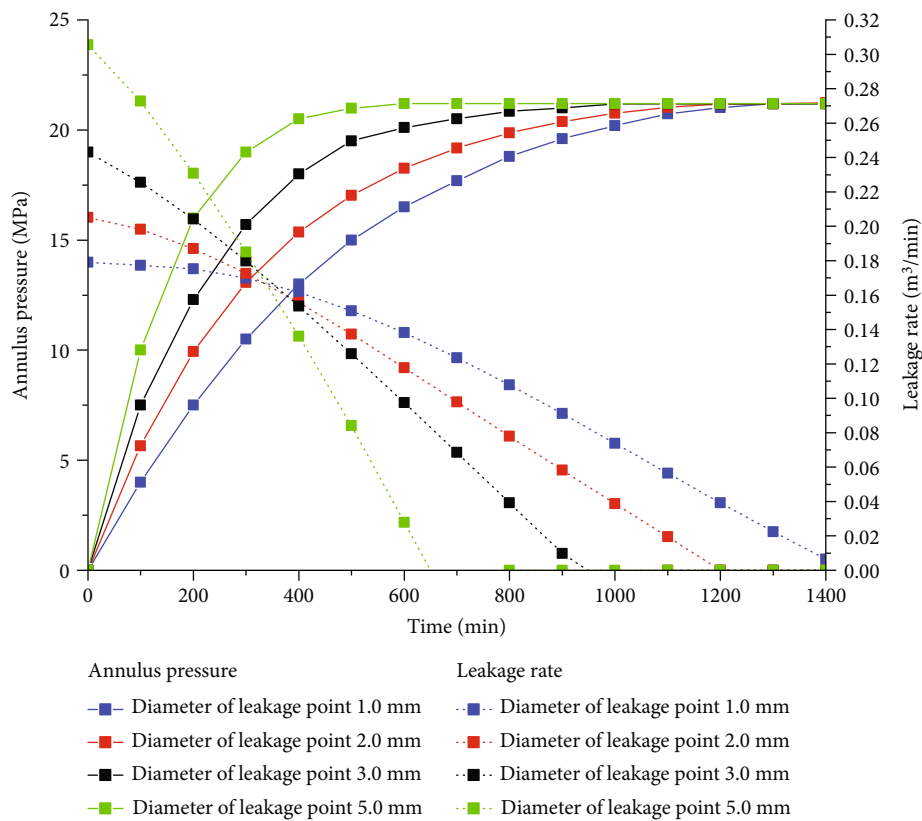

FIGURE 5: Circumferential pressure and leakage rate variation law under different leakage point orifice diameter.

TABLE 2: Characteristics and risks of different annulus starting pressure modes.

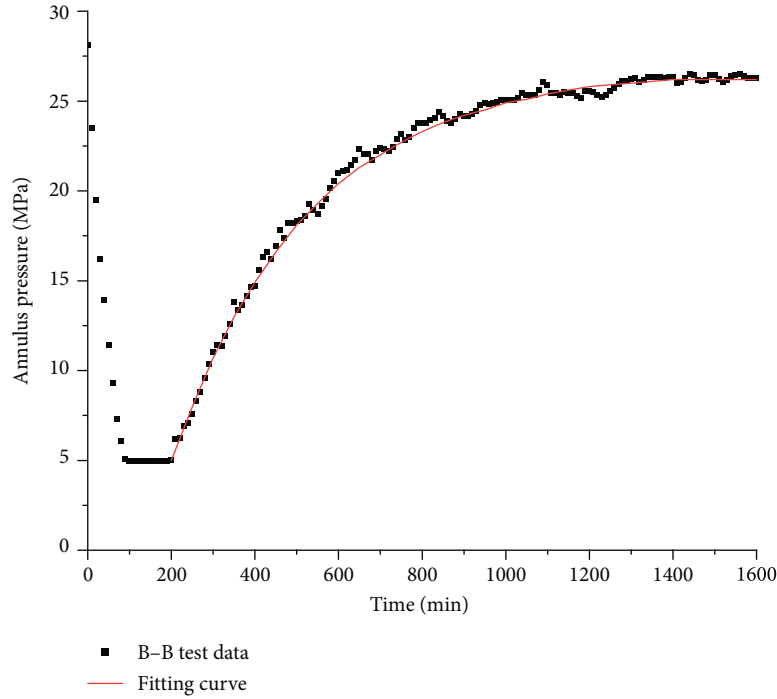| Number	Leakage point pore size	Leakage point depth	Maximum pressure value	Pressure rise rate	Pressure rise cycle	Accumulated gas volume	Risks
1	Big	Light (color)	High	Fastest	Shorter	Big	High
2	Small	Light (color)	High	Slow	Longest	Big	Medium
3	Big	Deep	Low	Soon	Minimum	Small	Medium
4	Small	Deep	Low	Slowest	Longer	Small	Low

FIGURE 6: Annular pressure relief/recovery testing curve of case well.

pressure rose to 21.24 MPa within 1400 min, of which the rate of pressure rise was faster in the first 500 min, and the volume of annulus gas grew faster. This shows that the continuous annular pressure can lead to the accumulation of a large amount of gas in the annulus, and the risks caused by gas accumulation should be paid attention to in the field operation. At the same time, the gas leakage changes with time from critical leakage to noncritical leakage, and the leakage rate remains high and basically unchanged during the critical leakage stage and gradually decreases during the noncritical leakage stage.

As shown in Figure 4, the depth of the leak point influences both the process of pressure rise in the annulus and the rate of leakage. At the early stage of pressure generation, the rate of rise of the annular pressure caused by different depth leak points is basically the same, after which the sustained annular pressure caused by shallow leak points has the characteristics of fast rise rate, long pressure rise period, and high-pressure value. The shallow leakage point has the characteristics of rapid annular pressure rise, long pressure rise period, and high-pressure value, which is caused by the long duration of noncritical leakage phase of shallow leak point. Taking the four curves of

1000 m, 2000 m, 3000 m, and 4000 m depth leak points in Figure 4 as an example, the highest-pressure value at the leak point is 23.3 MPa and the lowest is 15.2 MPa, respectively. The above analysis shows that the sustained annular pressure caused by the shallow leak point is more hazardous than the deep leak point.

As shown in Figure 5, the highest values of the sustained annular pressure under different leak point aperture conditions did not change, but the sustained annular pressure in the case of larger apertures rose quickly and had a short rise period, and the initial value of its leakage rate was large and fell quickly. The above analysis shows that the increase in leak point orifice diameter will not change the final pressure value but will lead to a significant increase in the leak rate and pressure rise. The above analysis shows that the increase in the diameter of the leak point will not change the final pressure value but will lead to a significant increase in the leak rate and pressure rise rate.

According to the above analysis, the depth of the leak point and the hole size are two important factors that affect the pressure rise process and the leak rate. According to the depth of the leak point and the size of the leak point

pressure, the pressure mode of the annulus can be divided into four categories: small-hole shallow leakage, small-hole deep leakage, large-hole shallow leakage, and large-hole deep leakage. As shown in Table 2, the four modes in the pressure value, pressure rise speed, pressure rise cycle, and amount of gas accumulation in the annulus have differences, taking into account the high-pressure value that affects the reliability of the wellbore safety barrier and pressure rise speed. Considering that a high-pressure value affects the reliability of the wellbore safety barrier, a fast pressure rise rate and a short rise period are unfavorable for early warning and control, and a larger volume of accumulated gas makes it more difficult to release the spray. The risks of the four models were evaluated qualitatively. Among them, the shallow leakage of large holes has the characteristics of high-pressure value, fast speed, and high gas volume, and its risk is the highest. In contrast, the small-hole deep leakage has the lowest risk. Therefore, extra attention should be paid to the integrity of the upper production tubular column of offshore gas wells to enhance its corrosion, tensile and compressive properties, and gas tightness to reduce the probability of shallow leakage from large boreholes.

Since the case well was put into production, the annulus sleeve pressure continued to rise. Testing was carried out using the annulus with pressure surface diagnostic device, and the components of annulus sample testing were basically the same as the gas phase components of the reservoir, so it was initially determined that the tubing was leaking. According to the construction requirements of B-B test, the annular pressure relief process was operated, as shown in Figure 6. The well annular pressure start-up pattern was consistent with the "small-hole shallow leakage" type characteristics, and the annular pressure was stable at about 23.0 MPa, with relatively high wellbore safety risk. Through fitting calculations, it was diagnosed that the pore size at the leak point of the well was 2.3 mm and the maximum leak rate was 0.30 m³/min, which was lower than the critical standard of 0.42 m³/min [16].

Due to the high difficulty of deep gas well annular pressure management and expensive well repair costs, the well-adopted ultrafine calcium carbonate leak plugging agent was used to reduce the degree of annular pressure fracture and regular injection of annular protection fluid to prevent stress corrosion and other methods to comprehensively manage annular pressure. The well has been able to ensure the smooth and safe production of gas.

5. Conclusions

(1) A model was developed to calculate the sustained annular pressure in the annular space of tubing-casing of an offshore high-temperature and high-pressure gas well with high CO_2. The analysis shows that the temperature and pressure differences between the inner and outer annuli of the tubular column provide the driving force for gas leakage generation. After the integrity failure of the tubular column, the annular pressure and gas volume gradually increase, but the rate of increase gradually slows down. As the pressure difference between the inside and outside of the leak point decreases, the leak rate gradually decreases, and the risk caused by gas accumulation should be considered in field operations

(2) The depth of the leak point and the hole diameter are two important factors that affect the pressure rise process and the rate of leakage. Circumferential pressure rise mode is divided into four categories: small-hole shallow leakage, small-hole deep leakage, large-hole shallow leakage, and large-hole deep leakage. Among them, large-hole shallow leakage has the characteristics of high-pressure value, fast speed, and high gas volume, and its risk is the highest, while small-hole deep leakage has the lowest risk. Therefore, extra attention should be paid to the integrity of the upper production tubular column of the offshore gas wells to enhance its corrosion resistance, tensile and compressive properties, and gas tightness to reduce the probability of shallow leakage from large boreholes

(3) The model involves only one leak point calculation method; in the actual working conditions, there may be multiple leak points in the oil pipe column, which will lead to more complex calculation of leak point depth, size, and leak rate; this model can be used as the superposition effect of multiple leak points and provide the judgment basis for the diagnosis of annular pressure on a macrolevel

Data Availability

The authors confirm that the data supporting the findings of this study are available within the article and its supplementary materials.

Conflicts of Interest

The authors declare that they have no conflicts of interest.

Acknowledgments

References

[1] B. Zhang, N. Lu, Y. Guo, Q. Wang, M. Cai, and E. Lou, "Modeling and analysis of sustained annular pressure and gas accumulation caused by tubing integrity failure in the production process of deep natural gas wells," *Journal of Energy Resources Technology*, vol. 144, no. 6, article 063005, 2022.

[2] T. Ma, Y. Tang, P. Chen, and Y. He, "Mitigation of annular pressure buildup for deepwater wells using a recovery relief method," *Energy Science & Engineering*, vol. 7, no. 5, pp. 1727–1747, 2019.

[3] L. Cao, J. Sun, B. Zhang, N. Lu, and Y. Xu, "Sensitivity analysis of the temperature profile changing law in the production string of a high-pressure high-temperature gas well considering the coupling relation among the gas flow friction, gas properties, temperature, and pressure," *Frontiers of Physics*, vol. 10, article 1050229, 2022.

[4] X. Xuyue ChenDu, J. Yang, D. Gao, Y. Zou, and Q. He, "Developing offshore natural gas hydrate from existing oil & gas platform based on a novel multilateral wells system: depressurization combined with thermal flooding by utilizing geothermal heat from existing oil & gas wellbore," *Energy*, vol. 258, article 124870, 2022.

[5] J. Yang, S. Wu, G. Tong et al., "Acoustic prediction and risk evaluation of shallow gas in deep-water areas," *Journal of Ocean University of China*, vol. 21, no. 5, pp. 1147–1153, 2022.

[6] Q. Yin, J. Yang, M. Tyagi et al., "Downhole quantitative evaluation of gas kick during deepwater drilling with deep learning using pilot-scale rig data," *Journal of Petroleum Science and Engineering*, vol. 208, article 109136, 2022.

[7] H. Zhiqiang, Y. Jin, and L. Shujie, "Prediction model of multilayer casing annular pressure buildup based on casing-cement sheath-formation with thermo-structural coupling effects," *Journal of Engineering Thermophysics*, vol. 39, no. 8, pp. 1824–1832, 2018.

[8] *Recommended Practice for Design Installation Repair and Operation on Subsurface Safety Valve System: SY/T 10024-1998*, China National Offshore Oil Corporation, Beijing, 1998.

[9] R. Xu and A. K. Wojtanowicz, "Pressure buildup test analysis in wells with sustained casing pressure," *Journal of Natural Gas Science and Engineering*, vol. 38, pp. 608–620, 2017.

[10] Y. R. Feng, A. Q. Fu, J. D. Wang et al., "Failure control and integrity technologies of tubing/casing string under complicated working conditions: research progress and prospect," *Natural Gas Industry*, vol. 40, no. 2, pp. 75–82, 2020.

[11] B. Zhang, Z. C. Guan, N. Lu, A. R. Hasan, Q. Wang, and B. Xu, "Trapped annular pressure caused by thermal expansion in oil and gas wells: a review of prediction approaches, risk assessment and mitigation strategies," *Journal of Petroleum Science and Engineering*, vol. 172, pp. 70–82, 2019.

[12] Z. Q. Hu, J. Yang, B. Lu et al., "Hydrostatic pressure characteristics and pressure control mechanism of foam casing in deepwater wells," *Acta Petrolei Sinica*, vol. 40, no. 6, pp. 726–733, 2019.

[13] L. Li, J. Yang, Y. Song et al., "Numerical study of the mud loss in naturally fractured oil layers with two-phase flow model," *Journal of Petroleum Science and Engineering*, vol. 210, article 110040, 2022.

[14] B. Zhang, Z. C. Guan, Q. Zhang, and H. A. N. Dong, "Prediction of sustained annular pressure and the pressure control measures for high pressure gas wells," *Petroleum Exploration and Development*, vol. 42, no. 4, pp. 567–572, 2015.

[15] H. Zhiqiang, L. Baoping, H. Xutian, Y. A. N. G. Jin, Y. A. N. G. Shunhui, and H. E. Hanping, "Surface diagnosis technology for the key parameters of leakage point in the tubing-casing annulus of deep gas wells," *Oil Drilling & Production Technology*, vol. 42, no. 5, pp. 632–636, 2020.

[16] Z. H. A. N. G. Bo, L. U. O. Fangwei, S. U. N. Bingcai, X. I. E. Junfeng, X. U. Zhixiong, and L. I. A. O. Hualin, "A method for wellbore integrity detection in deep oil and gas wells," *Petroleum Drilling Technology*, vol. 49, no. 5, pp. 114–120, 2021.

[17] Q. Yin, J. Yang, M. Tyagi et al., "Machine learning for deepwater drilling: gas-kick-alarm classification using pilot-scale rig data with combined surface-riser-downhole monitoring," *SPE Journal*, vol. 26, no. 4, pp. 1773–1799, 2021.

[18] API RP90, *Management of Sustained Casing Pressure on Offshore Wells*, American Petroleum Institute, Washington, 2006.

[19] W. Fu, Z. Wang, L. Chen, and B. Sun, "Experimental investigation of methane hydrate formation in the carboxmethylcellulose (CMC) aqueous solution," *SPE Journal*, vol. 25, no. 3, pp. 1042–1056, 2020.

[20] X. Chen and D. Gao, "The maximum-allowable well depth while performing ultra-extended-reach drilling from shallow water to deepwater target," *SPE Journal*, vol. 23, no. 1, pp. 224–236, 2018.

[21] S. H. I. Xiaolei, G. A. O. Deli, and W. A. N. G. Yanbin, "Predictive analysis on borehole temperature and pressure of HTHP gas wells considering coupling effect," *Oil Drilling & Production Technology*, vol. 40, no. 5, pp. 541–546, 2018.